Inorganic-Filler Chemical Vapor Deposition: A New Approach To Grow Nanoporous Thin Films

P. M. Parthangal and M. R. Zachariah*

Department of Mechanical Engineering and Department of Chemistry and Biochemistry, University of Maryland, College Park, Maryland 20742

A new method for the growth of nanoporous thin films is described. The process is targeted to the formation of titanium dioxide (TiO_2) through a low-temperature inorganic-filler chemical vapor deposition (CVD) process. The growth technique employs gas-phase reaction of an alkali metal (Na) and a metal halide ($TiCl_4$) and subsequent thin film growth within a low-pressure coflow diffusion reactor. Titanium and salt were codeposited from the gas phase on a heated graphite substrate placed within the reaction zone. After deposition, salt was removed from the surface through a water rinse, yielding a nanoporous structure. The remaining thin film was oxidized to yield titanium dioxide. Qualitative analysis of surface nanostructure and quantitative analysis of pore characteristics showed that the films contained TiO_2 in both anatase and rutile phases, with porosities ranging between 55 and 67%. The dependence of film thickness and pore characteristics on reactant velocity, substrate temperature, and reactant concentration are presented. The synthesis scheme should be generic to the formation of a wide variety of metal and metal oxide porous thin films.

Introduction

One of the current trends in the application of chemical vapor deposition (CVD) is the development of low-temperature processes both for energy efficiency considerations and to enable the use of a wider variety of substrates. Refractory metals and metal oxides in particular tend to require the use of relatively high temperatures (e.g., over 900 °C for thermal CVD of titanium).[1] Other desirable characteristics include the use of nontoxic reactants and minimization of hazardous byproducts of reaction.

In conjunction with the desire to have low-temperature processing, one of the architectures of recent interest is the formation of porous thin films. Several methods, such as spin coating, sol−gel processing, PVD, and CVD have been explored for the formation of interlayer dielectrics.[2,3] Porous materials with ordered micropores such as zeolites have been widely used as catalysts, adsorbents, and various supporting materials.[4]

In this work we focus on the production of nanoporous TiO_2 thin films, as a test case of a low-cost, low-temperature inorganic-filler CVD route that we will outline in this paper. Thin films of TiO_2 have been grown in the past using techniques such as metal−organic CVD (MOCVD) and sol−gel processes.[5−7] The production of high surface area TiO_2 is motivated by its photocatalytic activity and its application in the decomposition of organic compounds.[8] Previous studies of the photoactivity of nanosized TiO_2 particles have shown a dependence on surface area, particle size distribution, porosity, and crystal structure.[9] TiO_2 in both anatase and rutile crystal forms have been found to possess significant photocatalytic properties under different conditions.[10] Photocatalytic activity (PCA) is the ability of a material to create an electron−hole pair as a result of exposure to ultraviolet radiation. The control of PCA is important in many applications utilizing TiO_2, including paint pigments and cosmetics that require low PCA. The PCA of TiO_2 in thin coatings has also exhibited self-cleaning and disinfecting properties under exposure to UV radiation. The advantage of using a nanoporous TiO_2 thin film is that the high surface area over a flat surface provides for higher potential PCA.[11]

Basic Approach. The strategy used to produce porous thin films in this work is as follows. Two components, A and B, are produced in the gas phase through a chemical reaction and codeposited on a substrate to form a uniform thin film. Component B is then selectively removed from the thin film through some physical mechanism, leaving a porous thin film of A on the substrate. More specifically, we react alkali metal

* Corresponding author. E-mail: mrz@umd.edu.

(1) Hocking, M. G.; Vasantasree, V.; Sidky, P. S. *Metallic and Ceramic Coatings: High-Temperature Properties and Applications;* John Wiley and Sons: New York, 1989.

(2) Lee, H. J.; Lin, E. K.; Bauer, B. J.; Wu, W.; Hwang, B. K.; Gray, W. D. *Appl. Phys. Lett.* **2003**, *82* (7), 1084.

(3) Yim, J.-H.; Lyu, Y.-Y.; Jeong, H.-D.; Song, S. A.; Hwang, I.-S.; Hyeon-Lee, J.; Mah, S. K.; Chang, S.; Park, J.-G.; Hu, Y. F.; Sun, J. N.; Gidley, D. W. *Adv. Funct. Mater.* **2003**, *13* (5), 382.

(4) Corma, A. *Chem. Rev.* **1997**, *97*, 2373; Harris, K. D.; Brett, M. J.; Smy, T. J.; Backhouse, C. *J. Electrochem. Soc.* **2000**, *147*, 2002.

(5) Bernardi, M. I. B.; Lee, E. J. H.; Lisboa-Filho, P. N.; Leite, E. R.; Longo, E.; Souza, A. G. *Ceramica* **2002**, *48* (308), 192.

(6) Hotsenpiller, P. A. M.; Wilson, G. A.; Roshko, A.; Rothman, J. B.; Rohrer, G. S. *J. Cryst. Growth* **1996**, *166*, 779.

(7) Tracey, S. M.; Hodgson, S. N. B.; Ray, A. K.; Ghassemlooy, Z. *J. Mater. Proc. Technol.* **1998**, *77*, 86.

(8) Chu, S.-Z.; Wada, K.; Inoue, S.; Todoroki, S. *Chem. Mater.* **2002**, *14* (1), 266.

(9) Coronado, J. M.; Maira, A. J.; Conesa, J. C.; Yeung, K. L.; Augugliaro, V.; Soria, J. *Langmuir* **2001**, *17*, 5368. Yeung, K. L.; Yau, S. T.; Maira, A. J.; Coronado, J. M.; Soria, J.; Yue, P. L. *J. Catal.* **2003**, *219*, 107.

(10) Nosaka, Y.; Kishimoto, M.; Nishino, J. *J. Phys. Chem. B* **1998**, *102* (50), 10279. Bakardjieva, S.; Šubrt, J.; Štengl, V.; Večerníková, E.; Bezdička, P. *Solid State Phenomena* **2003**, *90−91*, 7.

(11) Fujishima, A.; Hashimoto, K.; Watanabe, T. *TiO2: Photo catalysis Fundamentals and Applications;* BKC Inc.: Tokyo, 1999.
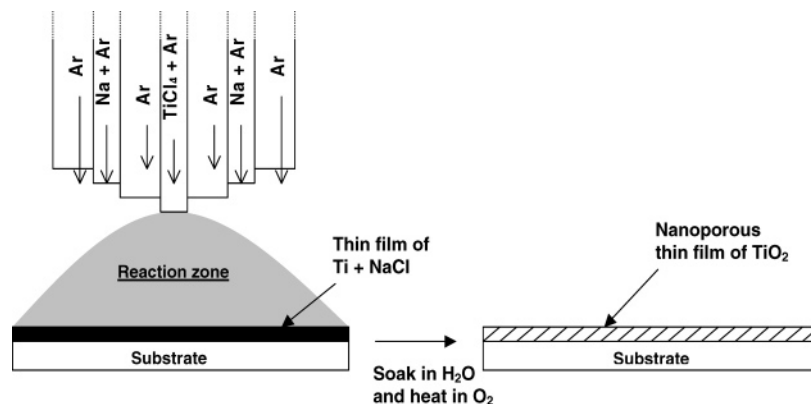
Figure 1. Schematic representation of experimental approach.

Table 1. CVD Reactor Conditions^a

| sample code | substrate temp (°C) | diluting Ar(g) (sccm) | | Ar(g) into bubbler (sccm) | | flow into reactor | | av reactant gas velocity (m/s) |
		mixed with Na	mixed with TiCl$_4$	Na	TiCl$_4$	Na(g) ($\times 10^{-6}$ mol/min)	TiCl$_4$(g) ($\times 10^{-7}$ mol/min)	
v1	400	205	20	30	0.22	1.54	3.41	4
v2	400	265	25	30	0.22	1.54	3.41	5
v3/t3	400	325	30	30	0.22	1.54	3.41	6
t1	380	325	30	30	0.22	1.54	3.41	6
t2/c3	390	325	30	30	0.22	1.54	3.41	6
c1	390	325	30	26	0.20	1.33	3.10	6
c2	390	325	30	28	0.21	1.44	3.25	6

^{a} Chamber pressure = 6 Torr, net diluting Ar(g) flow through reaction zone = 2.25 slpm, deposition time = 3 h in all cases, substrate diameter = 1.5 in.

vapor with a metal halide. The reaction is highly exothermic and generally spontaneous, yielding zerovalent metal and the corresponding alkyl halide, represented by the following equation:

$$mn\text{Na} + n\text{MX}_m \xrightarrow{\text{Ar}} \text{M}_n + nm\text{NaX}$$
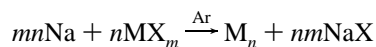
For our particular case, sodium was reacted with titanium tetrachloride. We have previously developed this chemistry to demonstrate low-temperature deposition of refractory compounds, where we operated under conditions where the vapor pressure of the salt was higher than the saturation vapor pressure at the substrate temperature.[12] This ensured that no salt would deposit in the film. More recently we developed a method to create ultrahigh surface area metal oxide nanoparticles using salt as a removable filler.[13]

In this work, we combined these two concepts, by allowing the salt to incorporate during the film deposition process, such that subsequent removal of the salt matrix left behind a porous film, as diagrammed in Figure 1. The advantage of the approach is that the salt acts as a crude templating medium that is highly economical and recyclable. The basic chemistry for the production of titanium, which involves the reaction of a metal halide and an alkali metal, is generic. This implies that many metal halides, and combinations thereof, can be employed. Furthermore, this class of chemistry is highly exothermic, implying a low-temperature deposition capability.

Experimental Section

A. Film Growth. The global reaction for the formation of a thin film of titanium and salt is

$$4\text{Na}(g) + \text{TiCl}_4(g) \xrightarrow{\text{Ar}} \text{Ti}(s) + 4\text{NaCl}(g)$$
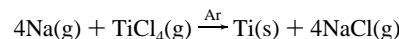
Na has a very high reductive power and strips Cl atoms from TiCl$_4$ via a facile series of reactions, resulting in the formation of Ti and NaCl in the gas phase, which in turn deposit and nucleate on the substrate surface. In this work, the reactants (Na and TiCl$_4$) were introduced in the gas phase along with argon into a coflow diffusion reactor maintained at a low pressure (6 Torr) and containing a heated graphite substrate. The specifics of the experimental system are detailed elsewhere.[12] After film deposition, the salt was removed with a water rinse, resulting in a porous thin film of Ti followed by oxidation to produce TiO$_2$.

The reactor conditions for the series of experiments conducted are listed in Table 1. Vapor pressures of both reactants were calculated at their respective operating temperatures (400 °C for Na and 22 °C for TiCl$_4$),[15] from which the mole fraction and hence molar concentration of each reactant entering into the chamber was calculated. The velocities of reactant gases entering the reaction chamber were controlled by the amounts of diluting argon mixed with the reactant gases prior to the nozzle inlet. Argon flow rates through the inner shroud of the nozzle separating the reactants and the outer shroud were kept constant at 250 sccm (standard cubic centimeters per minute) and 2 slpm (standard liters per minute), respectively (both equivalent to ~15 m/s). The former prevented reaction from occurring immediately below the nozzle, while the latter confined the reaction zone to the area above the substrate and enabled a streamlined flow of gases through the reactor. On

(12) Hendricks, J. H.; Aquino, M. I.; Maslar, J. E.; Zachariah, M. R. *Chem. Mater.* **1998**, *10*, 2221.
(13) Kim, S. H.; Liu, B. Y. H.; Zachariah, M. R. *Chem. Mater.* **2002**, *4* (7), 2889; Kim, S. H.; Liu B. Y. H.; Zachariah, M. R. *Langmuir* **2004**, *20*, 2523.

(14) Yaws, C. L. *Handbook of Vapor Pressure;* Gulf Publishing Co.: Houston, TX, 1995.
(15) Steffens, K. L.; Zachariah, M. R.; DuFaux, D. P.; Axelbaum, R. L. *Chem. Mater.* **1996**, *8* (8), 1871.
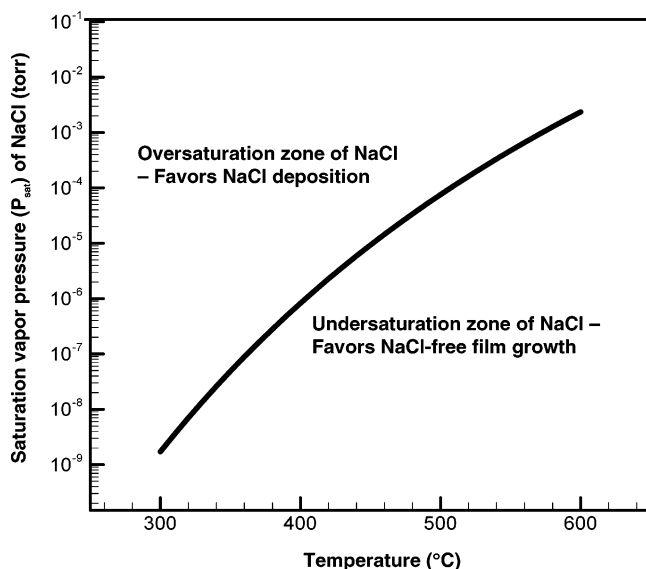
Figure 2. Variation of saturation vapor pressure of NaCl with temperature.[14]

the basis of the value of the saturation vapor pressure (P_{sat}) of NaCl at a given temperature (plotted in Figure 2), reactant concentrations entering the reaction chamber were adjusted such that the partial pressure of salt (P_p) produced by reaction exceeded P_{sat}. At the low working temperatures used in this CVD process (<400 °C), Ti has no significant vapor pressures, and hence, any Ti produced by reaction was assumed to deposit. Whenever reactant concentrations were reduced such that $P_p < P_{sat}$, only Ti was observed to deposit. The molar ratio of Na to $TiCl_4$ concentrations entering the chamber was always kept slightly higher than the stoichiometric requirement of 4.0 to ensure complete reduction of all chlorides within the reaction zone (see Table 1).[15]

Since the partial pressure of salt resulting from reaction was set to be higher than the saturation vapor pressure, homogeneous nucleation in the gas phase resulting in salt particles was a concern. However, since the production of salt was also linked to the sluggish reduction rate of the lower chlorides, we assumed that salt deposited on the surface almost entirely from the gas phase. Before beginning each experiment, the graphite substrates were polished using silicon carbide paper of different grits. A small amount of silver paste was applied to the bottom surface of the substrate, to ensure good thermal contact between the substrate and the heater surface. The chamber was then pumped down; the substrate was heated to the desired temperature; gaseous species were introduced into the chamber, and the deposition was carried out for about 3 h. The substrate was then allowed to cool to room temperature under a constant flow of argon before being removed from the chamber. Following salt removal, the sample was dried inside the reaction chamber, which was completely evacuated and brought up to atmospheric pressure with a constant 1 slpm flow of dry oxygen (99.995% pure). The sample was then heated to 400 °C for about 30 min to convert Ti into TiO_2.

B. Characterization and Pore Structure. Film microstructures, before and after salt removal, were examined with an SEM (JEOL JSM 6500 Field-Emission Gun SEM) while EDX determined their elemental composition (Ti, Na, Cl, and O). To assess the extent of salt deposition, chloride analysis was carried out using a Dionex DX 120 ion-chromatograph. Films were soaked in ultrapure, deionized water for about 48 h to dissolve the deposited salt from the film. The solution was then analyzed to quantify the amount of salt deposited. To characterize the pore structure, we used a combination of specular X-ray reflectivity (SXR) and Rutherford backscattering (RBS), while the crystal structure of films after oxidation was analyzed through X-ray diffraction (XRD).

At an X-ray wavelength of a few tenths of a nanometer, the refractive index of most materials is less than 1. Hence, there exists a critical grazing incidence angle at which the X-rays are totally reflected from the surface of the material.[16] This critical angle, θ_c, may be approximated by $(\rho r_e \lambda^2/\pi)^{1/2}$, where ρ refers to the electron density of the material, r_e (=2.818 fm) is the classical electron radius, and λ is the incident X-ray wavelength. All the angles defined in this process are grazing incidence angles measured from the surface parallel. Interference fringes occur due to constructive and destructive interference between X-rays reflected from the air/ film surface and the film/substrate interface at high incidence angles ($\theta > 2\theta_c$). The period of these fringes ($\Delta\theta$) is inversely proportional to the layer thickness, given by the relation $t = \lambda/2(\Delta\theta)$. This turns out to be an extremely convenient method to measure film thickness nondestructively.

The SXR measurements were done using a Philips high-resolution diffractometer, which consisted of a horizontal goniometer with a 2.2 kW sealed copper X-ray source. The incident beam was conditioned with a four-bounce germanium [220] monochromator, and specular data was collected with a grazing incident angle equal to the detector angle, ranging from 0.01° to 0.35° in the $2\theta-\omega$ configuration. The motion of the goniometer was controlled by a closed-loop active servo system with an angular reproducibility of 0.0005°. RBS measurements, performed on an MAS 1700 pelletron tandem ion accelerator, produced an estimate of the elemental composition of the porous film. The XRD patterns were obtained using a Siemens D500 diffractometer operating in the reflection mode with Cu Kα radiation (40 kV, 40 mA) and a diffracted beam monochromator, using the step scan mode for 2θ in the range of 20−60°, step size of 0.03°, and dwell time of 2 s per step.

The porosities of samples were computed once the amounts of salt and film thickness were known, since salt was the only leachable material for pore formation. We used a two-phase model to describe the porous material, where one phase comprised the voids and the other comprised the connecting material. The material between voids, i.e., the pore wall material, was assumed to be of uniform density. Mass densities of films were computed by combining electron density values from SXR and chemical composition values from RBS, which in turn was utilized to calculate pore wall densities of the films.

Results and Discussion

All experimental runs are summarized in Tables 1 and 2. Table 1 summarizes the process parameters used for each CVD experiment (e.g. flow rate, concentrations), while Table 2 summarizes results relevant to understanding the pore structure. In general, for this study we varied substrate temperature, the concentration of reactants, and the gas velocity into the reactor to vary residence time. The dynamic range of process parameters available to us was primarily limited by the nature of our sodium delivery system.

A. Characterization Prior to Salt Removal. We begin looking at the nascent films prior to salt removal using SEM and EDX. SEM images of sample v1, which was grown at a substrate temperature of 400 °C, are shown in Figure 3. The reactants entered the reactor with a linear gas velocity of 4 m/s and had a nominal residence time of 10 ms. The surface of the film appeared to have a uniform base structure of characteristic dimension ∼0.5 μm and some larger structures, which appeared to sit on top of the base structure

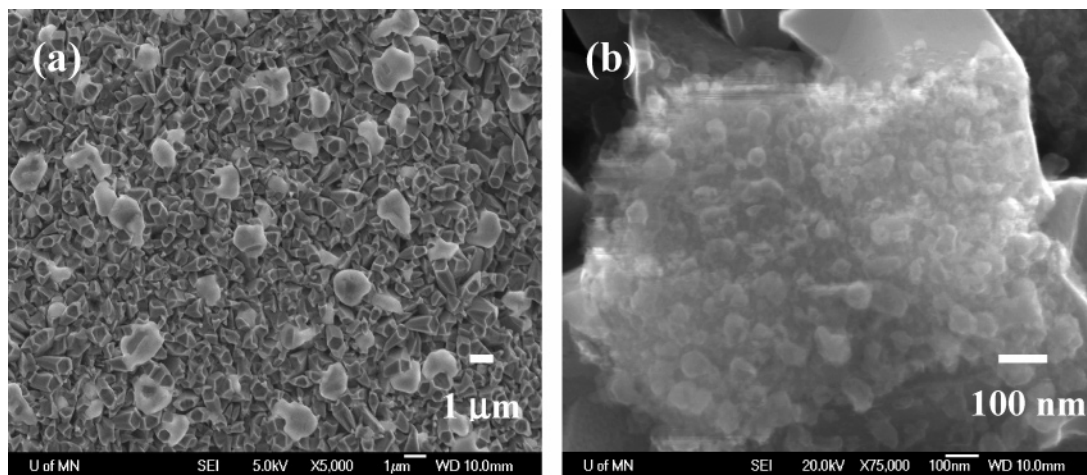(16) Lekner, J. *Theory of reflection;* Nijhoff: Dordrecht, 1987.

Figure 3. (a) SEM image of sample v1 (reactant inlet velocity = 4 m/s) indicates a uniform base structure with diamond-shaped crystallites of titanium, and aggregates of salt spread over the surface. (b) High magnification image of salt aggregate (acceleration voltage of electron beam = 20 kV) reveals titanium enclosed within salt matrix.

Table 2. Pore Structure Characterization

| sample code	NaCl mass (mg)	critical angle θ_c (deg)	Ti (%)	O (%)	Fe (%)	film thickness (μm)	porosity (%)	electron density ($\times 10^{32}$ e$^-$/m^3)	mass density (kg/m^3)	pore wall density (kg/m^3)
v1	1.373	0.105 00	34.2	63.0	2.8	0.87	63.3	1.59	553	1507
v2	1.495	0.111 25	33.6	63.6	2.8	0.97	62.2	1.78	618	1635
v3/t3	1.618	0.112 25	33.2	64.8	2.0	1.07	60.9	1.82	629	1609
t1	1.276	0.107 00	32.0	65.6	2.4	0.92	55.5	1.65	571	1283
t2/c3	1.487	0.112 00	32.1	66.2	1.7	1.01	59.5	1.81	626	1546
c1	1.395	0.100 00	32.5	64.8	2.7	0.85	66.8	1.44	499	1503
c2	1.428	0.102 50	33.1	65.3	1.6	0.92	62.8	1.51	525	1411
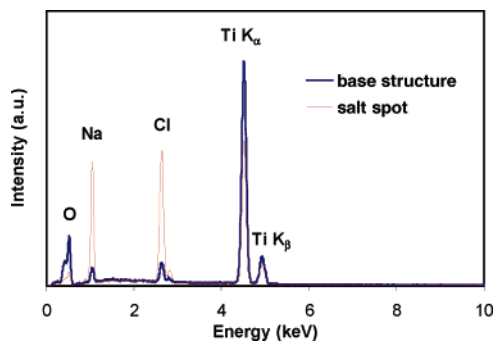
Figure 4. EDX spectra of sample v1 (reactant inlet velocity = 4 m/s) from two different regions, one on the base structure and the other on a salt aggregate.

with characteristic dimensions of about ∼1 μm. A closer look at the base revealed diamond-shaped crystallites. EDX analysis of the base surface indicated two peaks for titanium (indicating two phases) and peaks for oxygen, sodium, and chlorine, as seen in Figure 4. The base structure was assumed to be predominantly titanium, and the mounds were assumed to be primarily of salt. Focusing a high-energy electron beam (SEM acceleration voltage of 20 kV) on one of the mounds induced melting of the salt and clearly revealed titanium particles embedded in the salt matrix (corresponding to Figure 3b). The EDX analysis at this spot resulted in much higher intensity peaks for sodium and chlorine, as also shown in Figure 4. Figure 5 illustrates the surfaces of samples v2 and v3, where the average gas velocities of reactants were 5 and 6 m/s, respectively. Clearly, the salt structures were diminished in size and much more evenly dispersed over the film surface in comparison with the structures on sample
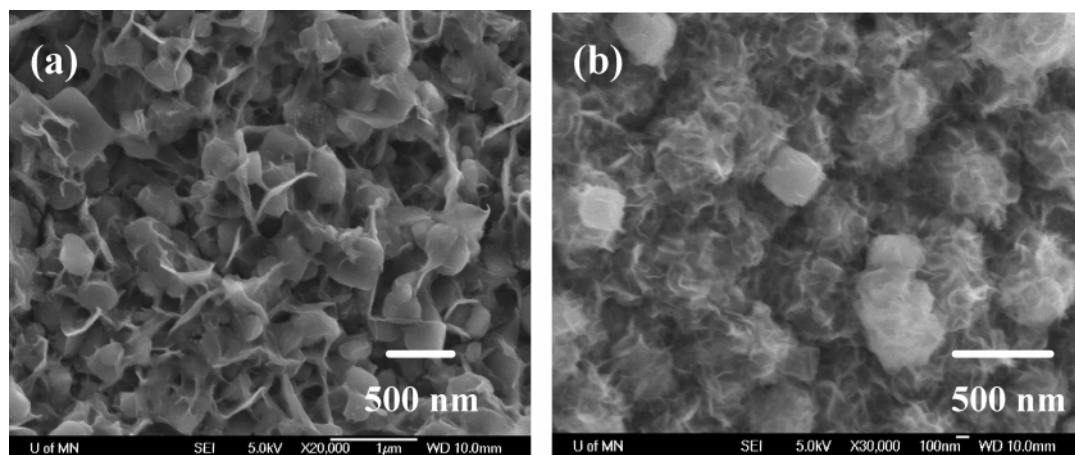

Figure 5. (a) SEM image of sample v2 (reactant inlet velocity = 5 m/s) indicates a uniform base structure along with the appearance of "streams" connecting salt aggregates. (b) SEM image of sample v3 (reactant inlet velocity = 6 m/s) clearly shows an increased density of salt streams on the surface.
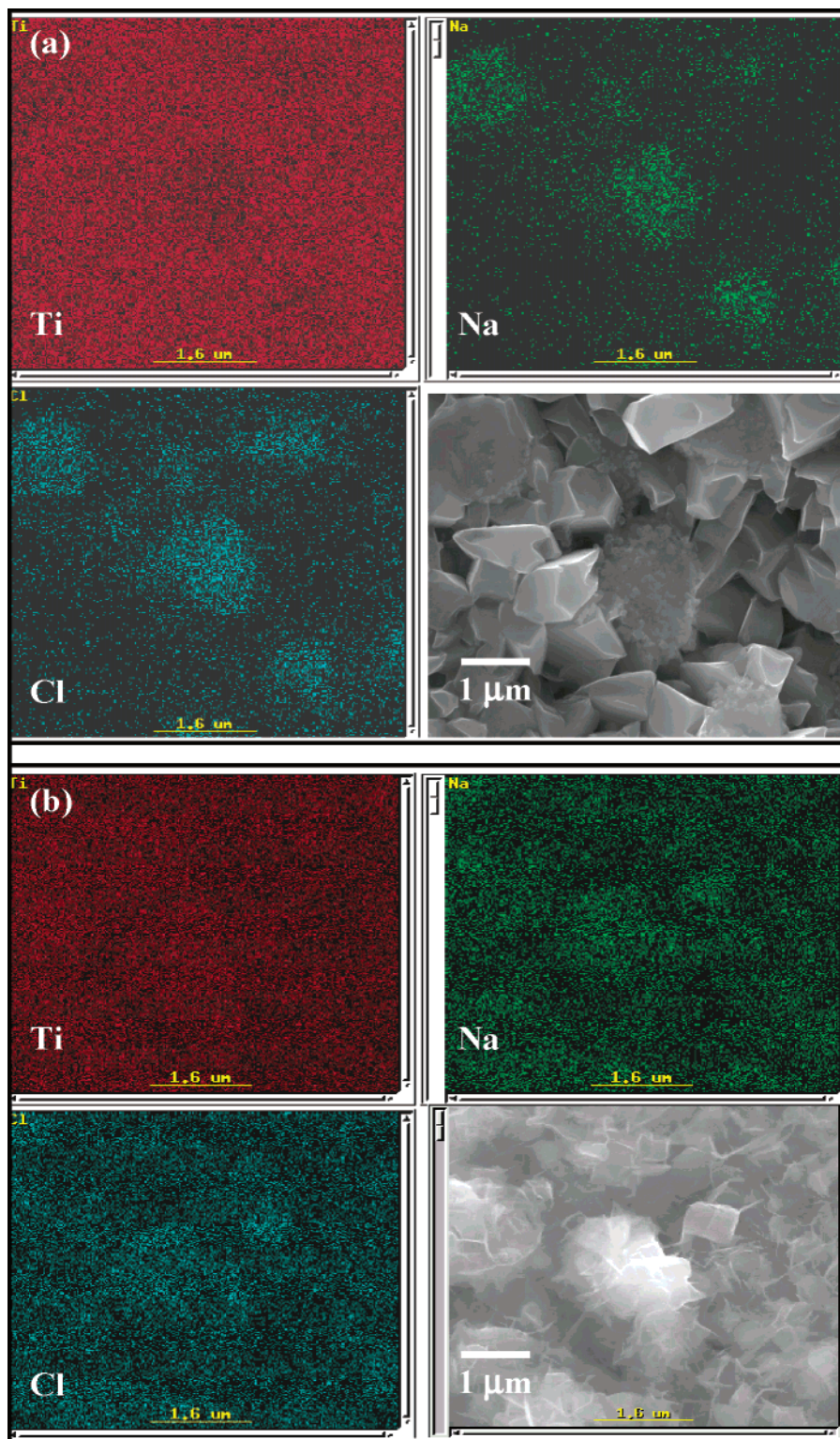
Figure 6. X-ray maps of Ti, Na, and Cl. Clockwise from bottom left, Cl, Ti, and Na SEM image; the scale bar applies for maps as well as SEM image. (a) X-ray elemental mapping for sample v1 (reactant inlet velocity = 4 m/s) shows a nearly uniform distribution of Ti over the entire surface, while Na and Cl are confined to salt aggregates. (b) Map for sample v3 (reactant inlet velocity = 6 m/s) suggests a more uniform distribution of Na and Cl over the entire substrate surface.

v1. We also observed the appearance of several structures that look like frozen liquid streams on the surface, presumably connecting salt aggregates. The density of these salt streams was seen to increase with increasing inlet velocity of reactants.

X-ray elemental mapping for samples v1 and v3 are shown in Figure 6. This confirmed that the mounds indeed contained a much higher concentration of sodium and chlorine and that with increasing flow velocity (sample v3) the salt was more homogeneously dispersed. Similarly, with increasing substrate temperatures and higher reactant concentrations, the salt was more evenly distributed on the film surface.

The salt removal experiments, where the aqueous salt solutions were analyzed by ion chromatography, were used
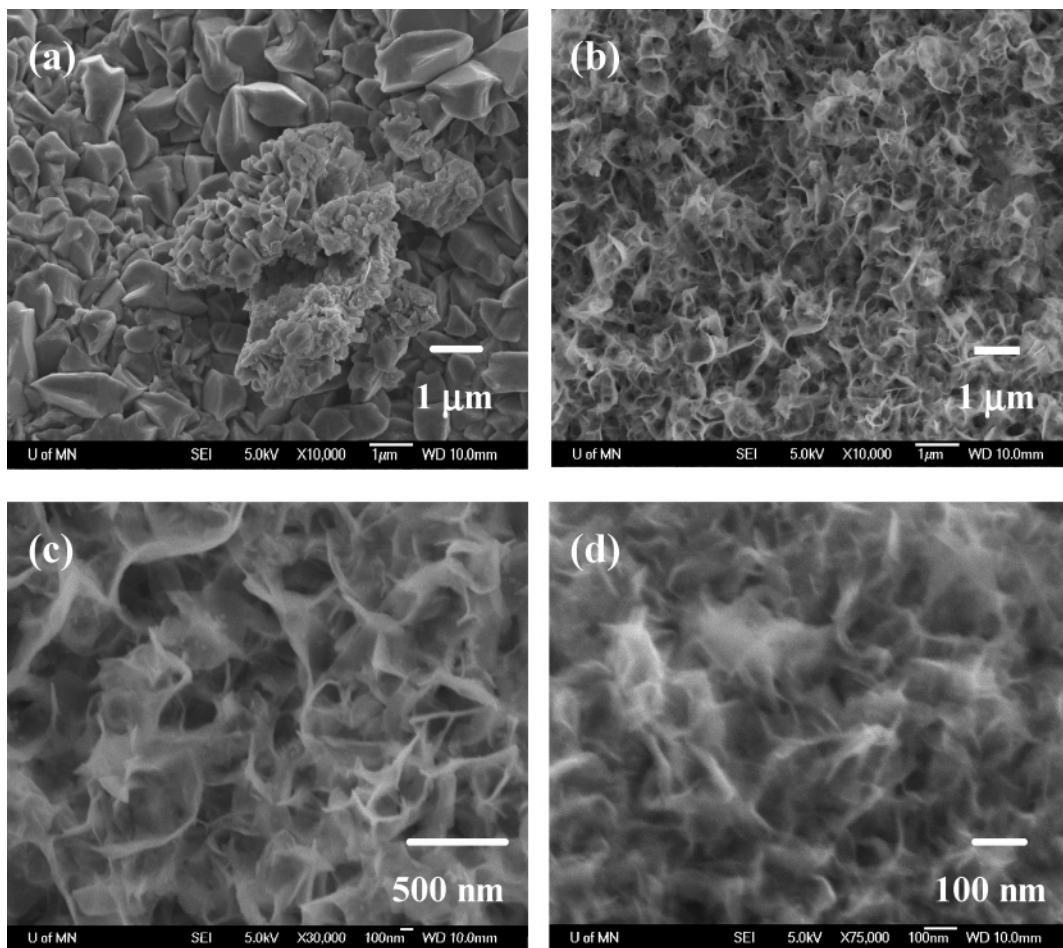
Figure 7. SEM images of samples after salt removal. (a) Sample v1 (reactant inlet velocity = 4 m/s): salt aggregates are no longer present, and there is a residue of titanium left behind in the regions where salt was removed. (b and c) Sample v2 (reactant inlet velocity = 5 m/s): highly porous film left behind after salt removal. (d) Sample v3 (reactant inlet velocity = 6 m/s).

to quantify the amount of salt incorporated in the substrates listed in Table 2. The amount of salt deposited was seen to increase for increasing gas flow velocity, substrate temperature, and reactant concentrations. An increase in the inlet velocity of reactants corresponds to a higher mass loading of reactants into the reaction zone, resulting in higher product formation. At higher substrate temperatures, surface reaction kinetics is enhanced, resulting in higher deposition rates of Ti and NaCl.

B. Characterization following Salt Removal. Next we look at the morphology and composition of films following salt removal. SEM images are shown in Figure 7. The absence of salt was confirmed through EDX analysis on various spots on sample v1, as shown in Figure 8. Similarly, EDX analysis of other samples also confirmed that salt was removed from all samples. A simple visual inspection of the micrographs indicated that all samples were highly porous. At this juncture, we confirmed that the experiments were indeed successful in producing nanoporous titanium thin films on the graphite substrates.

The critical grazing incidence angles from SXR measurements for different samples are listed in Table 2. The electron densities of the samples were calculated on the basis of the value of these angles and are tabulated in Table 2, along with a list of film thicknesses. The elemental composition of the samples was estimated using RBS. It was found that
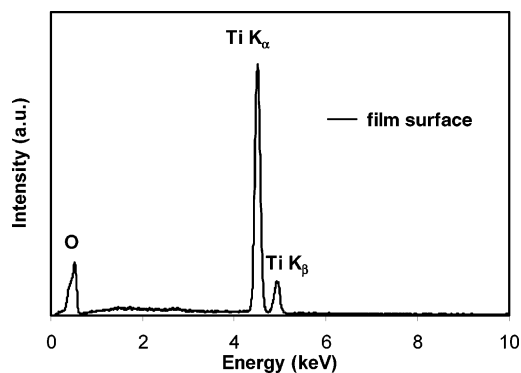

Figure 8. EDX spectrum of sample v1 (reactant inlet velocity = 4 m/s) after removal of salt shows the absence of Na and Cl and peaks for Ti and O.

all samples contained trace amounts of iron (Fe), which was most probably an impurity associated with the reactant carrier lines in the experimental setup, due to the corrosive nature of Na and $TiCl_4$. The tabulated amounts were measured and fitted using an in-built software package, "HYPRA", to extract the individual concentrations of elements present. Table 2 lists the values calculated for all samples, reflecting the dominant presence of titanium and oxygen with ratios close to the stoichiometric value for TiO_2. The elemental composition from RBS combined with electron density data from SXR was used to calculate the mass density and pore

wall density of the films.

From our study, we observed that both film thickness and the total amount of salt incorporated into the film increased with increasing reactant velocities, substrate temperature, as well as reactant concentration. The ratio of amounts of products incorporated into the thin film to the thermodynamically calculated amounts, for given inlet reactant concentrations, was found to be in the range of 60−70% for Ti and 8−10% for NaCl. The porosity was seen to decrease at higher reactant velocities and higher reactant concentrations, indicating that the amount of salt deposited relative to titanium decreased under these conditions. The porosity was found to increase for higher substrate temperature, however, this trend will change because the amount of salt deposited will gradually reduce to zero above a substrate temperature of 600 °C, since the partial pressure of salt will fall below P_{sat}.[12]

A typical XRD pattern from the surface of sample v3/t3 (reactant inlet velocity = 6 m/s, substrate temperature = 400 °C), seen in Figure 9, shows TiO_2 in a mixture of anatase (predominantly, with mean crystallite size of 15.1 nm) and rutile phases. Polycrystalline anatase has been proven to be an excellent photocatalyst for the mineralization of 4-chlorophenol in aqueous solution.[10]

Conclusions

In summary, we have demonstrated a simple, efficient process to produce and characterize nanoporous metal and metal−oxide thin films at relatively low operating temperatures. By suitable adjustment of experimental parameters such as the substrate temperature, reactant concentration, and the amounts of diluting gases, we ensure that conditions are conducive for deposition of salt in addition to the metal. The salt may be exclusively removed so that a porous metal film
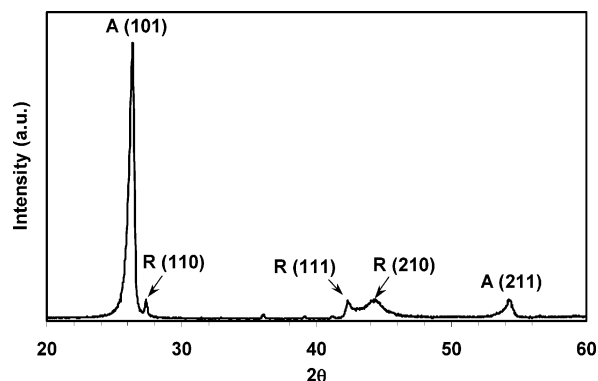

Figure 9. XRD pattern of sample v3/t3 (reactant inlet velocity = 6 m/s) after oxidation indicates peaks for anatase (A) and rutile (R).

remains. Since the pores result from removal of salt, the amount of salt deposited on the film corresponds directly to the pore volume.

Nanoporous thin films of titanium dioxide, with porosities in the 55−67% range, were grown. The films were extensively characterized to describe surface microstructure, film thickness, elemental composition, crystal structure, and pore characteristics. Film thickness was seen to increase with increasing reactant inlet velocity, substrate temperature as well as reactant inlet concentrations. The porosity decreased with increasing reactant velocity and concentration but was observed to increase with increasing temperature. The experimental scheme described here is generic in nature, and should be amenable to generate a wide variety of nanoporous metals and nonmetals, as well as metal oxides.